FINAL REPORT

Grant Title: Nonlinear Localized Dissipative Structures for Long-Time Solution of Wave Equation

By
Dr. John Steinhoff
Grant number: FA9550-05-0354

AFRL-SR-AR-TR-09-0291

REPORT DOCUMENTATION PAGE

PLEASE DO NOT RETURN YOUR FORM TO THE ABOVE ORGANIZATION.

1. REPORT DATE *(DD-MM-YYYY)*	2. REPORT TYPE	3. DATES COVERED *(From - To)*
28-07-2009	Final Technical Report	15 May 2005-30 Nov 2008

4. TITLE AND SUBTITLE
A LOCAL PARABOLIC METHOD FOR LONG DISTANCE WAVE PROPAGATION

5a. CONTRACT NUMBER

5b. GRANT NUMBER
FA9550-05-1-0354

5c. PROGRAM ELEMENT NUMBER

6. AUTHOR(S)
John Steinhoff, PhD

5d. PROJECT NUMBER

5e. TASK NUMBER

5f. WORK UNIT NUMBER

7. PERFORMING ORGANIZATION NAME(S) AND ADDRESS(ES)
The University of Tennessee Space Institute
411 B. H. Goethert Parkway
Tullahoma, TN 37388-9700

8. PERFORMING ORGANIZATION REPORT NUMBER

9. SPONSORING/MONITORING AGENCY NAME(S) AND ADDRESS(ES)
Office of Naval Research
100 Alabama Street, SW; Suite 4R15
Atlanta, GA 30303-3104

10. SPONSOR/MONITOR'S ACRONYM(S)

11. SPONSOR/MONITOR'S REPORT NUMBER(S)

12. DISTRIBUTION/AVAILABILITY STATEMENT
~~Public Release~~
Distribution A

13. SUPPLEMENTARY NOTES

14. ABSTRACT

A new numerical method, "Wave Confinement" (WC), is developed to efficiently solve the linear wave equation. This is similar to the originally developed "Vorticity Confinement" method for fluid mechanics problems. It involves modification of the discrete wave equation by adding an extra nonlinear term that can accurately propagate the pulses for long distances without numerical dispersion/diffusion. These pulses are propagated as stable codimension-one surfaces and do not suffer phase shift or amplitude exchange in spite of nonlinearity. The pulses remain thin unlike conventional higher order numerical schemes, which only converge as N (number of grid cells across the pulse) becomes large. The additional term does not interfere with conservation of the important integral quantities such as total amplitude, centroid. Also, properties like varying index of refraction, diffraction, multiple reflections are included and tested.

15. SUBJECT TERMS
WAVE CONFINEMENT, WAVE EQUATION, SOLITARY WAVES

16. SECURITY CLASSIFICATION OF:			17. LIMITATION OF ABSTRACT	18. NUMBER OF PAGES	19a. NAME OF RESPONSIBLE PERSON
a. REPORT	b. ABSTRACT	c. THIS PAGE			John Steinhoff
					19b. TELEPHONE NUMBER *(Include area code)* 931-393-7467

Abstract

A new numerical method, "Wave Confinement" (WC), is developed to efficiently solve the linear wave equation. This is similar to the originally developed "Vorticity Confinement" method for fluid mechanics problems. It involves modification of the discrete wave equation by adding an extra nonlinear term that can accurately propagate the pulses for long distances without numerical dispersion/diffusion. These pulses are propagated as stable codimension-one surfaces and do not suffer phase shift or amplitude exchange in spite of nonlinearity. The pulses remain thin unlike conventional higher order numerical schemes, which only converge as N (number of grid cells across the pulse) becomes large. The additional term does not interfere with conservation of the important integral quantities such as total amplitude, centroid. Also, properties like varying index of refraction, diffraction, multiple reflections are included and tested.

The generated short pulses can be best described as solitary waves, which can recover the shape after a collision due to nondestructive interaction between the pulses. Within the pulse, the dissipative effects due to the numerical errors are balanced with those of nonlinearity and the pulse will its their original form and speed even after many collisions. The pulse is also used as a carrier wave to propagate other properties such as direction. Wave equation solutions in the high frequency approximation can be generated using the carrier wave approach. WC, together with Keller's Approximation is then used to capture diffraction effects from a straight edge.

Scattering over complex bodies can be modeled with no use of complicated adaptive grid generation schemes around the bodies. The confinement term smoothens the boundary and prevents stair casing effects but the boundary remains thin. Validation studies have been performed for a number of real flow models and compared to the exact solutions. It is observed that the solutions match quite well with the exact solution.

1. INTRODUCTION

The main objective of this dissertation is to develop a new and efficient algorithm to accurately solve the linear wave equation. The idea comes from an already existing method "Vorticity Confinement" (VC), which was developed for a vast range of fluid dynamics problems [1]. Hence, the new method "Wave Confinement" (WC) is named after the existing approximation (VC). The linear wave equation can describe different classes of wave phenomena. Such classes include acoustics, electro-magnetics, microwave theory, etc. This dissertation focuses on scalar wave propagation over long distances. Effects to be accommodated include variation of the index of refraction, multiple scattering from complex surfaces, and some cases of diffraction.

2. APPROACH

2.1 Introduction

Let us consider a scalar field, ϕ, which satisfies the one sided wave equation (advection equation) advecting with constant speed c:

$$\frac{\partial \phi}{\partial t} + c\frac{\partial \phi}{\partial x} = 0 \qquad 2.1$$

Evidently, if the above equation is numerically solved using a conventional, discrete finite difference scheme, it tends to develop discretization errors. The conventional Eulerian schemes [8] suffer dissipation no matter what the order is. Many higher order schemes have been proposed to reduce the numerical diffusion/dispersion, but they only reduce the error if the number of grid points across the pulse, N is relatively large. As the present work involves treating thin pulses ~ 2–3 grid cells in size, the method is not necessarily going to be more accurate with increasing order. To keep the pulse confined on the discrete domain, numerical dissipation/dispersion must be counter-acted by adding a new term to the advection equation that will not interfere with the essential properties of the pulse. This term is called the "Confinement" term and hence the method is named "Wave Confinement" (WC). Ideas of adding extra terms to prevent numerical dissipation were previously proposed by Harten [9] to capture 1D contact discontinuities in compressible flows. The discretized form can only conserve a limited number of physical quantities of the pulse corresponding to the limited number of grid nodes across the pulse. Here, these are taken to include total amplitude at each grid point and the centroid speed. The modified form of equation (2.1) with the confinement term is then

$$\frac{\partial \phi}{\partial t} = -c\frac{\partial \phi}{\partial x} + E \qquad 2.2$$

where, $E = \dfrac{\partial^2 F}{\partial x^2}$. The idea is that the second order form of F acts as a "pulse shaping" term and, as long as $F \to 0$ as $|x| \to \infty$, the quantities of interest are conserved. A simple form of F can be taken as

$$F = \mu'\phi - \varepsilon'\Phi, \qquad 2.3$$

where μ', ε'. Here, constants and Φ is the harmonic mean given as

$$\Phi(x) = \frac{3}{\dfrac{1}{\phi(x-h)} + \dfrac{1}{\phi(x)} + \dfrac{1}{\phi(x+h)}}, \qquad 2.4$$

where h is the distance between two points, which tends to zero in the continuous limit. The confinement term is chosen such that it acts as an "expansion" or positive diffusion for shorter wavelengths and a "contraction" or negative diffusion for longer wavelengths. Also, the method must have a nonlinear term, otherwise some modes will decouple and diverge. The nonlinear term prevents the amplitude to escape to long wavelengths and can keep the pulse confined to a few grid cells.

2.2 WC as a Nonlinear Partial Differential Equation

To better understand the properties of the WC method, the harmonic mean, Φ, given in equation (2.4) is approximated as a partial differential equation. The Taylor expansions for $\phi(x+h)$ and $\phi(x-h)$ to second order are

$$\begin{aligned}\phi(x+h) &= \phi(x) + h\phi'(x) + \frac{h^2}{2!}\phi''(x), \\ \phi(x-h) &= \phi(x) - h\phi'(x) + \frac{h^2}{2!}\phi''(x),\end{aligned} \tag{2.5}$$

where $\phi' = \partial_x \phi$, $\phi'' = \partial_x^2 \phi$. By substituting the Taylor expansions into equation (2.4), and neglecting the higher order terms, the nonlinear term, Φ, is then approximated as

$$\Phi = \phi - \frac{2h^2}{3}\left(\frac{\phi'^2}{\phi}\right) + \frac{h^2\phi''}{3} + h^4\left(\frac{\phi'^4}{3\phi^3} + \frac{\phi'^2\phi''}{3\phi^2}\right), \tag{2.6}$$

where $h \to 0$ in continuous limit and terms of the order h^4 can be neglected. Using equation (2.6), equation (2.2) becomes

$$\partial_t \phi = -c\partial_x \phi + \partial_x^2\left(-\alpha\phi - \lambda\partial_x^2\phi + 2\lambda\frac{(\partial_x\phi)^2}{\phi}\right), \tag{2.7}$$

where $\alpha = \varepsilon' - \mu'$, $\lambda = \frac{\varepsilon' h^2}{3}$. All the parameters, μ', ε', α, and λ, are chosen to be positive. When $\phi = 0$, the above equation fails but, it is important to note that the discretized form of equation (2.7) used for computations is given in equation (2.17). The harmonic mean in equation (2.21) is still finite for $\phi = 0$.

Equation (2.7) describes the conservation of the following integral quantities:
total amplitude,

$$A_T = \int \phi dx, \tag{2.8}$$

and centroid speed,

$$\frac{d\hat{x}}{dt} = \frac{\int \phi c dx}{A_T}, \tag{2.9}$$

where $\hat{x}$ is the centroid, given by

$$\hat{x} = \frac{\int x\phi dx}{A_T}. \tag{2.10}$$

It is important to note that all the terms in equation (2.7) are homogenous of degree one unlike many non-linear equations, which use non-homogenous terms for the nonlinear term [10]. Thus, the confinement does not depend on the scale of the quantity to be convected (which is, of course, a property of the original linear equation (2.1)). Defining the confinement term in the equation (2.7) as the sum of three terms gives,

$$E = E_0 + E_1 + E_2 , \qquad 2.11$$

where $E_0 = -\alpha\partial_x^2\phi$, $E_1 = -\lambda\partial_x^4\phi$, and $E_2 = 2\lambda\partial_x^2\left(\frac{(\partial_x\phi)^2}{\phi}\right)$. It is interesting that the role of the second order term (E_0) in equation (2.11) is different from typical nonlinear pde's studied, such as KdV, that harbor solitary waves: In these, the linear second order term is the "expansion" term, and the "contraction", or "steepener" term is the nonlinear Burgers-like convection: $(\partial_x\phi^2/2)$. In WC, the linear second order term, E_0, *contracts* the pulse and the nonlinear term, E_2, prevents ϕ from changing sign and transfers amplitude from long wavelength to short, and the fourth order term, E_1, acts as a diffusion for short wavelengths and prevents the solution from diverging. The amplitude imparted to the field by the WC terms remains confined and propagated as stable wave packets without dispersion/diffusion. The appearance of ϕ in the denominator of equation (2.7) makes E_2 diverge as $\phi \to 0$. This prevents ϕ from changing sign. Since the total amplitude, A_T, is conserved, the integral of ϕ over any finite region cannot then diverge. In the discretized version defined in Section 2.3, none of the grid values can diverge in appropriate ranges of α and λ. This ensures realizability if ϕ is a physical quantity. Smolarkiewicz [11] also has rearranged the discretized convection equation so that there is such a term in the denominator for this reason.

By rearranging the terms, equation (2.7) may be expressed as

$$\partial_t\phi = -c\partial_x\phi + \partial_x^2\left(\frac{1}{\psi^2}\left(-\alpha\psi + \lambda\partial_x^2\psi\right)\right), \qquad 2.12$$

where $\psi = 1/\phi$. In the convecting frame, $\xi = x - ct$, the above pde simply reduces to the heat equation,

$$\partial_t\phi = \partial_\xi^2 F \qquad 2.13$$

where $F = \frac{1}{\psi^2}\left(-\alpha\psi + \lambda\partial_\xi^2\psi\right)$. At convergence, $F \to 0$, and therefore reduces to

$$-\alpha\psi + \lambda\partial_\xi^2\psi = 0 . \qquad 2.14$$

It can be seen that the above equation is similar to the simplest form of Sturm-Liouville eigenvalue equation with $\beta = \sqrt{\alpha/\lambda}$. The solution to the equation (2.14) will then be of the form,

$$\psi = C_1\left(e^{\beta x} + e^{-\beta x}\right). \tag{2.15}$$

Then the solution for ϕ is

$$\phi = A\operatorname{sech}\left[\beta(\xi)\right], \tag{2.16}$$

where C_1, C_2 and A are arbitrary constants.

2.3 Discretization

Using first order upwind in time and second order centered in space, the discretized form of equation (2.2) is written as

$$\phi_j^{n+1} = \phi_j^n - \frac{\nu}{2}\left(\phi_{j+1}^n - \phi_{j-1}^n\right) + \delta_j^2 F_j^n \tag{2.17}$$

where $\delta_j^2 F_j^n = F_{j+1}^n - 2F_j^n + F_{j-1}^n$, $\nu = \dfrac{c\Delta t}{h}$, Δt is the time step and h is the grid cell size. Even on the discrete domain, the confinement term, F, conserves the essential quantities such as total amplitude,

$$A_T = \sum_{j=1}^{J} \phi_j = \text{const}, \tag{2.18}$$

and centroid speed,

$$v = \langle j \rangle^n - \langle j \rangle^{n-1} = \frac{\sum_{j=1}^{J} j\phi_j^n - \sum_{j=1}^{J} j\phi_j^{n-1}}{A_T}, \tag{2.19}$$

where J is the total number of grid points. The confinement term F is defined as

$$F_j^n = \mu\phi_j^n - \varepsilon\Phi_j^n, \tag{2.20}$$

where $\mu = \dfrac{\mu'\Delta t}{h^2}$, $\varepsilon = \dfrac{\varepsilon'\Delta t}{h^2}$, μ' is a diffusion coefficient and ε' is the confinement coefficient. ε' along with μ', control the width and rate of convergence of the pulse, and Φ is the nonlinear harmonic mean of N (including N–1 neighboring nodes) grid points. For 1D, N =3, and,

$$\Phi_j^n = \left[\frac{\sum_{l=-1}^{+1} (\phi_{j-l}^n)^{-1}}{3} \right]^{-1} . \qquad 2.21$$

Equation (2.17) would simply reduce to the Euler explicit form, which is unconditionally unstable when $\varepsilon = 0$ and $\mu = 0$. The two (positive) parameters, ε and μ, are determined by the requirements for convergence, such that the small features relax to their solitary wave shape in a small number of time steps and can have an effective support (to have a significant magnitude) of a small number of grid cells. In the semi-discrete limit, the scalar field ϕ relaxes to a definite shape as derived in Section 2.3.1. In the moving frame ($\nu = 0$), equation (2.17) reduces to a discrete heat equation,

$$\phi_j^{n+1} = \phi_j^n + \delta_j^2 F_j^n \qquad 2.22$$

that simulates the stationary pulse. At convergence, the positive and negative artificial dissipation terms are balanced with the nonlinearity to produce stable pulses that can stay confined and structurally stable to numerical perturbations (caused, for example, by the discrete convection term or another wave passing through).

2.3.1 Convergence

At convergence, $\delta_j^2 F \to 0$, $F \to 0$ and $(\mu\phi - \varepsilon\Phi) \to 0$. If N = 3 in the harmonic mean, the equation for F at a point is

$$\mu\left(\frac{1}{\phi_{j-1}} + \frac{1}{\phi_j} + \frac{1}{\phi_{j+1}} \right) - \frac{3\varepsilon}{\phi_j} = 0 . \qquad 2.23$$

Solutions to equation (2.23) that satisfy the boundary conditions: $F \to 0$, $|j| \to \infty$ are of the form,

$$\phi \to A\,\mathrm{sech}\left[\gamma(j - j_0)\right], \qquad 2.24$$

where j_0 is the approximate position of the centroid. Here, γ is a pulse width coefficient and is determined by substituting equation (2.24) into (2.23):

$$\cosh\gamma = \left[\frac{1}{2}\left(\frac{3\varepsilon}{\mu} - 1 \right) \right] . \qquad 2.25$$

Furthermore, the above equation can be reduced to a quadratic form in e^{γ},

$$e^{2\gamma} - \left(\frac{3\varepsilon}{\mu} - 1\right)e^{\gamma} + 1 = 0, \tag{2.26}$$

for which the solution is

$$e^{\gamma} = \frac{b \pm \sqrt{b^2 - 4}}{2} \tag{2.27}$$

or

$$\gamma = \ln\left(\frac{b \pm \sqrt{b^2 - 4}}{2}\right), \tag{2.28}$$

where $b = \left(\frac{3\varepsilon}{\mu} - 1\right)$. The solution is real if $b^2 - 4 > 0$ and this requires that $\varepsilon/\mu \geq 1$. If $\varepsilon = 0$, F acts as a positive diffusion for all wavelengths and the solution decays. When $\mu = 0$, the solution becomes unstable even if $\varepsilon = 0$. So, a minimal amount of diffusion is essential for the stability purpose. If $\mu \leq \varepsilon$, F acts as negative diffusion for longer wavelengths so that the features remain confined and stable to perturbations against spreading.

2.4 Results

For the evaluation of the scheme and to demonstrate the efficient properties of the WC method, a number of tests are performed and presented. To show convergence, a single point pulse of arbitrary amplitude chosen to be 2,

$$\phi_j = \begin{Bmatrix} 2, & j = j_0 \\ 0, & j \neq j_0 \end{Bmatrix} at\ n = 0, \tag{2.29}$$

with parameters $\nu = 0$, $\varepsilon = 0.3$, $\mu = 0.2$ and $j_0 = 128$ is simulated on a grid of 256 points using periodic boundary conditions. The discretized equation used for this computation is

$$\phi_j^{n+1} = \phi_j^n + F_{j+1}^n - 2F_j^n + F_{j-1}^n. \tag{2.30}$$

When the solution reaches convergence, the pulse is relaxed to a hyperbolic secant given by equation (2.24). In Figure 2.1, the solid line is the algebraically calculated hyperbolic secant with width given by equation (2.28), and the points are computed using equation (2.30). For better comparison, the normalized function, ϕ/A is plotted against the hyperbolic secant. It can be clearly seen that the solution matches quite well with the analytically calculated hyperbolic secant. When discretized form of equation (2.1) is solved using a higher order method, the solution quickly spreads to a large number of grid points. It can be seen in Figure 2.2 that the

solution from a higher order method spreads by large amount after only 100 times steps, but the confinement method keeps the pulse compact.

3. FORMULATION

As in convection, a nonlinear term, E is added to the one dimensional full wave equation. The wave equation with confinement terms, that control the shape of the pulse, is

$$\partial_t^2 \phi = c^2 \partial_x^2 \phi + E \tag{3.1}$$

where $E = \partial_t \partial_x^2 F$. A simple discretization for the above pde will be

$$\phi_j^{n+1} = 2\phi_j^n - \phi_j^{n-1} + \nu^2 \delta_j^2 \phi + \delta_n^- \delta_j^2 F \tag{3.2}$$

where $\delta_n^- f = f^n - f^{n-1}$, $\delta_j^2 f_j = f_{j-1} - 2f_j + f_{j-1}$, $\nu = \dfrac{c\Delta t}{h}$, Δt is the time step and h is the grid cell size, and F is defined as in the advection case.

$$F_j^n = \mu \phi_j^n - \varepsilon \Phi_j^n \tag{3.3}$$

where $\mu = \dfrac{\mu' \Delta t}{h^2}$, $\varepsilon = \dfrac{\varepsilon' \Delta t}{h^2}$. At convergence (when the propagating pulse shape converges), the solution to the equation (3.2) is

$$\phi \to A_1 \operatorname{sech}\left(\gamma(j - j_0 + \nu n)\right) + A_2 \operatorname{sech}\left(\gamma(j - j_0 - \nu n)\right) \tag{3.4}$$

where A_2 and A_2 are arbitrary constants, j_0 is the initial position of the centroid and the pulse width coefficient, γ, is defined as in equation (2.28). Equation (3.4) describes two pulses moving forward and backward. It is shown in Section 2 that the addition of WC terms in the form of second derivatives of a function that has short range do not change the propagation speed or the total amplitude. The same is true for the wave equation, if an additional time derivative is applied. The main constraint on the confinement term, F, as in advection is that it forces an initial isolated, propagating short range pulse with single maxima to remain short range and also not develop any additional maxima. An important property of the wave equation is that it is linear. Therefore, properties of the computed solution should not depend on the amplitude. The behavior of solution computed using equation (3.1) is shown in Figure 3.1. When $\mu = 0$ and $\varepsilon = 0$, the solution becomes unstable. A little amount of diffusion ($\mu = 0.2$) will prevent the unstable behavior but the solution suffers large amount of spreading. Now, when the confinement term ($\varepsilon = 0.3$) is added, the pulse becomes stable and at the same time, remains thin. The dissipative/dispersive effects are balanced with those of the nonlinearity to produce stable localized structures [13].

3.2 Results

In this section, numerical examples are provided to confirm that no discretization errors are developed in the quantities of interest and that there is no significant spreading of the pulses during propagation. The formulation given by equation (3.4) is used for the numerical experiments. While analyzing the formal accuracy of the present scheme, a theoretical error estimate is beyond the scope, because the equation is nonlinear. However, evaluation of numerical error is done experimentally, and demonstrated that the scheme possesses the convergence that was discussed in the previous chapter.

3.2.1 Long-time propagation

To begin with, the propagation of pulses for long distances is observed. This is the idealization of waves without dissipation. Convergence analysis is illustrated by examining the behavior of a delta function as an initial pulse. Let the initial pulse be

$$\phi_j^n = \begin{Bmatrix} 2, & j = j_0 \\ 0, & j \neq j_0 \end{Bmatrix} \text{at } n = 0 \text{ and } n = 1 \tag{3.5}$$

where $j_0 = 128$ and the computation is done on 256 grid points. The pulse from WC is compared to the solution from a conventional higher order method and is shown in Figure 3.2. The two pulses in the plot are the forward and backward propagating scalar functions. It is obvious that WC preserves the thickness and total amplitude of the pulse with no significant numerical dissipation. Higher order methods do not help because increasing the order of the numerical scheme is only efficient when there are a large number of points across the propagating function.

3.2.2 Wave Interaction

Before moving to higher dimensions, the pulse interaction phenomenon is discussed to understand the performance of WC during multiple collisions of pulses. To represent interacting wave equation solutions, when pulses pass through each other, there must be no amplitude exchange or phase shift. Otherwise, the actual wave equation being studied could not be accurately simulated, since it is linear. However, a nonlinear term is required in the WC equation in order to create a solitary wave representation of the pulse, which will be non-diffusing when discretized. Interaction between soliton-like pulses is an important property, which has been studied for a long time using nonlinear equations [14]. It is more appropriate to only re-introduce the nonlinear pde for WC, which was derived in Section 2, to establish a relation to other existing nonlinear pde's. The nonlinear pde for WC is

$$\partial_t \phi = \partial_x^2 \left(-\alpha\phi - \lambda \partial_x^2 \phi + 2\lambda \frac{(\partial_x \phi)^2}{\phi} \right). \tag{3.7}$$

The above equation has a similarity to the Cahn-Hilliard (CH) equation, which describes the process of phase separation, by which the two components of a binary fluid spontaneously separate and form domains pure in each component. A simple form of the CH equation is

$$\partial_t \phi = \partial_x^2 \left(-\alpha_1 \phi - \alpha_2 \partial_x^2 \phi + \alpha_3 \phi^3 \right) \tag{3.8}$$

where α_1, α_1, α_1 are arbitrary, positive constants. The commonality includes the same linear terms and the appearance of a Laplacian in front of the non-linear term. This commonality is not surprising since the CH equation was one of the leading models proposed for a phenomenological description for a fluid interface and phase separation (decomposition into pure phases) [15]. The CH equation describes the evolution of concentrated fields (like thin pulses evolved from WC). Though the equations are similar, the resulting non-linear term is not exactly the same as in the commonly used form of the CH equation.

An important point is that other nonlinear pde's like Kdv, which can successfully propagate localized structures, suffer phase shift after collision [16]. This is not present in WC. For the new formulation used, this interaction effect vanishes. This vanishing is due to the fact that both the Laplacian and the time derivative operator operate on the nonlinear term.

The preservation of centroid speed during interaction is shown in Figure 3.3 for an initial condition given by equation (3.5). The centroid positions of forward and backward propagating pulses are plotted. Periodic boundary conditions are used for this simulation over a grid of 256 grid points. It can be noticed that even after many collisions, no jump in the centroid position is noticed after interaction. The importance of preserving the right speed plays a dominant role in generating constant phase surfaces, which will be discussed in Section 5. The same is true for preservation of total amplitude. In Figure 3.4, it can be seen that two pulses of different amplitudes are effectively transparent (after a short relaxation time) to one another and do not lose their amplitudes during collisions. For this computation, the initial conditions used are,

$$\phi_j^n = \begin{Bmatrix} 2, & j = j_{01} \\ 1, & j = j_{02} \\ 0, & j \neq j_{01} \text{ and } j \neq j_{02} \end{Bmatrix}. \qquad 3.9$$

The two initial pulses are first relaxed to hyperbolic secants of respective amplitudes using heat equation ($c=0$). So, the two initial conditions of the two pulses are then

$$\phi_j^n = \begin{Bmatrix} A_1 \operatorname{sech}\left[\gamma\left(j - j_{01}\right)\right] + A_2 \operatorname{sech}\left[\gamma\left(j - j_{02}\right)\right], & n = 0 \\ A_1 \operatorname{sech}\left[\gamma\left(j - j_{01} - v\right)\right] + A_2 \operatorname{sech}\left[\gamma\left(j - j_{02} + v\right)\right], & n = 1 \end{Bmatrix} \qquad 3.10$$

where $A_2 = \frac{A_1}{2}$, $j_{01} = 128$ and $j_{02} = 140$. The pulses are then propagated towards each other to observe the interaction between the pulses.

3.3 WC for higher dimensions

3.3.1 2D

In higher dimensions, WC behaves the same way as in 1D. The essential physics is accurately preserved as analyzed in Section 2. The discretized equation in 2D is

$$\phi_{i,j}^{n+1} = 2\phi_{i,j}^{n} - \phi_{i,j}^{n-1} + v^2 \nabla^2 \phi + \delta_n^- \left(\nabla^2 F\right) \qquad 3.11$$

where i is the grid index in x-direction, j is the grid index in y-direction and ∇^2 is the 2D extension of the discrete Laplacian used in 1D . For convenience the aspect ratio of the grid is 1. However, behavior of WC with different aspect ratios is studied in Section 4. The nonlinear factor, $\Phi^n_{i,j}$, in the confinement term F is

$$\Phi^n_{i,j} = \left[\frac{\left(\phi^n_{i\pm1,j}\right)^{-1} + \left(\phi^n_{i,j\pm1}\right)^{-1} + \left(\phi^n_{i,j}\right)^{-1}}{N} \right]^{-1} \tag{3.12}$$

where the number of terms in the sum, N = 5. Here, it is assumed that $\phi^n_{i,j} \geq 0$. Negative values can also be accommodated with a small extension. Both μ and ε are positive. Assuming convergence as $n \to \infty$ (for $\nu = 0$),

$$\nabla^2(\mu\phi - \varepsilon\Phi) = 0 \tag{3.13}$$

for which the solution at convergence is

$$\phi_{i,j} = A \sec h[\gamma(r_{i,j} - r_0)] \tag{3.14}$$

where

$$r_{i,j} = x_i \cos\theta + y_j \sin\theta \tag{3.15}$$

A, z_0, θ are constants, $x_i = ih$, $y_j = jh$, h is the grid cell size, and γ is the inverse pulse width. The solution converges to a straight pulse (in 2-D) concentrated about a line at angle, θ and at any position. By substituting the solution in equation (3.13), it is easy to see that γ satisfies

$$\frac{\varepsilon}{\mu} = [1 + 2ch(\gamma h\cos\theta) + 2ch(\gamma h\sin\theta)]/5. \tag{3.16}$$

The solution has translational invariance and γ depends (to a small extent) on orientation, θ. However, the centroid speed and amplitude in the normal direction is independent of θ as can be seen from equation (3.16). To demonstrate long distance propagation with no increasing numerical errors, a diverging circular wave of speed, $\nu = 0.23$ is simulated on a $(128)^2$ cell grid with periodic boundary conditions. Confinement values used were $\mu = 0.2$, $\varepsilon = 0.3$. The initial conditions for this computation are

$$\begin{aligned} \phi^{n=0}_{i,j} &= A_0 \sec h\left[\gamma r_{i,j}\right] \\ \phi^{n=1}_{i,j} &= \frac{A_0}{A_1} \sec h\left[\gamma\left(r_{i,j} - \nu\right)\right] \end{aligned} \tag{3.17}$$

where r is the radius of the wave. The actual wave equation exhibits a "tail" behind a pulse in 2-D, which can be seen to be suppressed by the Confinement, and, effectively, only the steep pulse front is accurately computed. In Figure 3.5, the circular wave for different time steps is presented. It can be seen that the wave persists on the grid for very long time. Also, as in 1-D, there is no discernable interaction between intersecting waves. The waves retain their form and orientation in spite of multiple head-on collisions.

3.3.2 3D

In 3D, the discretized form of the wave equation with the confinement term is

$$\phi^{n+1}_{i,j,k} = 2\phi^{n}_{i,j,k} - \phi^{n-1}_{i,j,k} + \nu^2\nabla^2\phi^{n}_{i,j,k} + \delta^{-}_{n}\left(\nabla^2 F^{n}_{i,j,k}\right) \qquad 3.18$$

where ∇^2 is the 3D extension of the discrete Laplacian used in 1D, and the nonlinear harmonic mean at a point, $\Phi^{n}_{i,j,k}$, is

$$\Phi^{n}_{i,j,k} = \left[\frac{\sum_{\alpha=-1}^{+1}\sum_{\beta=-1}^{+1}\sum_{\chi=-1}^{+1}\left(\phi^{n}_{i+\alpha,j+\beta,k+\chi}\right)^{-1}}{27}\right]^{-1}. \qquad 3.19$$

Long distance propagation in 3D is simulated for an expanding, initially spherical wave and is shown in Figure 3.6. The computation is done on a coarse, $(64)^3$ cell grid with periodic boundary conditions. The initial diameter for this computation is 32 grid cells. Confinement values used were $\mu = 0.2$ and $\varepsilon = 0.3$. As in the 2-D case, the wave remains completely confined. Unlike in 2D, the actual solution does not exhibit a tail behind the front and the solution corresponds to the full physical solution rather than just the wavefront. The solution at a given point *P(x, y, z)*, depends only on the information on the sphere and not on the interior of the sphere. Thus the interior of the sphere is a lacuna for the solution. It is true for odd numbers of space dimension.

4 WAVE FRONT PROPAGATION

4.1 Focusing

Focusing is the phenomenon of the waves converging on a point or line. This is important in studying caustic regions. A common situation where caustics are visible is when light shines on a drinking glass. Focusing phenomenon has been extensively applied in a variety of engineering, optics, computer graphics and medical applications. In caustic regions, many waves intersect. Fixed grid Eulerian methods have limits on the effective resolution due to the limited number of grid points in a caustic unlike Ray Tracing schemes [4] [17]. To overcome this problem, complex

schemes have been considered such as Osher's higher dimensional Liouville equation representation [18] and localization of caustics [19]. However, these seem to be complex and computationally costly.

It was first thought that, since during focusing, the number of grid points on the wave decreases, WC is not going to help to retain the information at focusing regions. It was later shown that WC accurately computes waves through caustic regions and is stable to discretization effects produced on the grid. Since the interest is in the long distance propagation, the detailed resolution at the focusing itself was not an issue and that focusing in intermediate regions does not interfere with the long distance wave propagation. In Figure 4.1, amplitude contours are compared to Lagrangian markers (exact solution in high frequency approximation). It can be seen that the wave contours match quite well with markers. Also, the basic information defined by the initial conditions is not lost, even though only the simple Eulerian algorithm was used, with no additional logic. Recent developments in level set methods can capture focusing regions [21]. However, these are computationally complex unlike WC.

4.2 Reflection from Complex Boundaries

The property of waves to reflect from boundaries is captured accurately using WC without having to use adaptive grids around the boundaries. This reflection of waves is responsible for echoes, interference, etc. The energy and momentum of the waves is reflected back with or without 180 degrees phase change depending on the properties of the boundary. The form of a reflected wave front is determined by those of the incident wave front and the surface. Boundaries many contain many irregularities and for short pulses (high frequency content), these irregularities can be larger than the wavelengths. Higher order discretization may be needed for conventional treatments of long distance propagation to reduce numerical diffusion in the propagation. Since WC does not have this diffusion problem, complex configurations can be accurately captured using very efficient, lower order discretizations with no loss of accuracy. A very effective method for treating reflections can then be implemented that does not require complex surface fitted grids, but allows the surface to be simply 'immersed' in a uniform Cartesian grid as shown in Figure 4.2. This method employs a "level set" representation of the surface and can easily accommodate very complex topography with little computational effort. For example, reflection from a boundary of function, $f(i, j) = 0$, is shown, where,

$$\phi_j^n = 0, \quad f \le 0, \text{ at all } n. \tag{4.1}$$

The effects of boundaries are smooth and no stair casing is observed. Reflection from complex terrains with many irregularities is important to capture interference effects in radio wave propagation. The irregularities can be very much larger than the wavelength of the short of waves that are propagated.

4.2.1 Scattering from Cylinder

Scattering is a physical process in which the direction of a wave deviates from its normal trajectory due to non-uniformities in the medium or interaction with boundaries. A wave packet with a bundle of rays parallel to each other will reflect in different angles if they encounter a non-

uniform obstacle (diffuse reflection or scattering). If such a bundle encounters a smooth surface such as mirror, the rays remain as bundle upon leaving the surface (specular reflection).

Scattering from the cylinder is diffuse reflection and is simulated accurately using WC. Consider the oblique incidence of a plane wave on a perfectly conducting infinite cylinder. The scalar field, ϕ, is set to zero inside the cylinder of radius 32 grid cells. The reflected surface is manipulated to re-direct or re-shape the plane wave front into a cylindrical scattered field. If the plane wave is polarized, the polarity is reversed when it encounters perfectly conducting obstacles or hard boundaries (This is not demonstrated here). The confinement term, F is diffusive in the tangential direction and contracting in the normal direction. This prevents stair-casing effects and generates a smooth scattered field, which can be seen in Figure 4.3. The scattered field does not quickly diffuse on the grid and can be detected near the receiver, which is located far away from the target. This is important in applications such as target detection. The scalar quantity, ϕ, is very sensitive and can be used to detect targets smaller than the grid cell size. When the field of computation is very large, the number of grid points across the target will be relatively small. The direct scattering problem involves determining the scattered field, which depends on the characteristics of the scatterer studied in this section for different cases. However, a lot of work is yet to be done in inverse scattering, which is considered for future research.

Before proceeding to the study of complex configurations of obstacles, a plane wave reflection from a sine wave boundary is computed and shown. The same can be effectively captured using WC and is shown in Figure 4.4. It can be seen that WC itself can capture the effects of the boundary.

4.3 Varying Index of Refraction

When a wave interacts with the medium of varying density, it refracts (scatters). Refraction can be described by Snell's law, which states that the angle of incidence is related to the angle of refraction.

$$\frac{\sin\theta_1}{\sin\theta_2} = \frac{v_1}{v_2} = \frac{n_2}{n_1} \tag{4.2}$$

where n_1, n_2 are the indices of refraction of the two layers of medium, θ_1, θ_2 are the angles of incidence and refraction respectively and v_1, v_2 are the speeds of the pulse in the respective layers. One example of refraction in the atmosphere is mirage.

In acoustics, refraction is the bending or curving of a sound ray that results when the ray passes through a sound speed gradient from a region of one sound speed to a region of a different speed. The amount of ray bending is dependent upon the amount of difference between sound speeds. For water, sound speed depends on the variation in temperature, salinity, and pressure of the water. Similar acoustics effects are also found in the Earth's atmosphere. The phenomenon of refraction of sound in the atmosphere has been known for centuries; however, beginning in the early 1970s, widespread analysis of this effect came into existence through the designing of urban highways and noise barriers to address the meteorological effects of bending of sound rays in the

lower atmosphere. Refraction of radio waves in evaporated ducts (formed due to variations in humidity near sea) and ionospheric ducts (formed due to variation in solar radiation) is important in radio wave propagation.

4.3.1 Profile of varying index of refraction: Converging waves

Consider a profile for varying speed,

$$v(j) = const * \exp(\alpha(j - j_0)^2), \tag{4.3}$$

which has maximum speed (v) at $j = j_0$. An isolated plane wave propagated across the medium with the profile given in equation (4.3) is computed. The discretized equation used for the wave propagation is,

$$\phi_{i,j}^{n+1} = 2\phi_{i,j}^{n} - \phi_{i,j}^{n-1} + \delta_i^2 v_j^2 \phi_{i,j}^{n} + \delta_j^2 v_j^2 \phi_{i,j}^{n} + \delta_n \left(\delta_i^2 F_{i,j}^{n} + \delta_j^2 F_{i,j}^{n}\right). \tag{4.4}$$

When the index of refraction is non-uniform, the waves tend to bend towards regions of higher index. It can be seen in Figure 4.8 that the computed pulses travel without diffusion and numerical errors in speed were insignificant to plottable accuracy. The computed pulse is compared to Langrangian markers (the blobs in Figure 4.5) for validation, which are calculated as,

$$\begin{aligned} x_{new} &= x_{old} + v s_{x,new} \\ y_{new} &= y_{old} + v s_{y,new} \end{aligned} \tag{4.5}$$

where s_x and s_y are the components of the propagating direction. The direction is updated according to the gradient in index of refraction on that marker as,

$$\begin{aligned} s_{x,\bullet} &= s_{x,old} \\ s_{y,\bullet} &= s_{y,old} - \frac{dv}{dy} \end{aligned} \tag{4.6}$$

and the normalized components of the direction are,

$$\begin{aligned} s_{x,new} &= \frac{s_{x,\bullet}}{\sqrt{s_{x,\bullet}^{\,2} + s_{y,\bullet}^{\,2}}} \\ s_{y,new} &= \frac{s_{y,\bullet}}{\sqrt{s_{x,\bullet}^{\,2} + s_{y,\bullet}^{\,2}}}. \end{aligned} \tag{4.7}$$

When the index of refraction is randomly varying and does not have a smooth profile, curve fitting methods must be used to fit the random variations. This becomes very complex when the index of variation is a function of time. But, for a smooth profile, the computation of markers is exact and is used for validation.

As shown in Figure 4.5, the pulse does not lose information in spite of the limited number of grid points across the focusing regions. However, Lagrangian markers suffer inadequacy in number of grid points and fail to maintain continuity.

4.3.2 Duct like profile used in EM propagation

Electromagnetic waves propagating in the atmosphere encounter regions of varying density, which cause bending of the waves. One example is the evaporation duct, which is associated with a sharp drop in moisture immediately above water bodies. The drop in moisture decreases the density and in turn increases the speed.
A predetermined profile of varying index of refraction, which imitates such a duct is treated:

$$\nu(j) = 0.23 - 0.0023 * |j - j_0| \qquad 4.10$$

where $j_0 = 30$. A curved surface configuration (for the ground) is employed, which is immersed in the uniform Cartesian grid. A plane wave propagating through the specified medium is shown in Figure 4.6. Lagrangian markers are also plotted for comparison purpose. The marker positions are computed as given in equations (4.5), (4.6), (4.7). It can be seen that the markers fail to maintain the continuous surface when the wave is diverging, but fall in the band of contours computed by WC.

4.4 Multiple grids

One other important use of WC for the wave equation involves cases with multiple grids with grid interfaces. This property plays an important role when a fine grid has to be used around the near field (source/antenna) and coarser grid in the far field. A fine grid is typically used near the antenna to resolve the high field gradients. To propagate the wave over long distances, a coarse grid scale must be used in the far field. The test case used only treats uniform grids, and not the antenna for illustration. If only the discretized wave equation is used, with no Confinement, reflections are produced from the grid interfaces, unless special care is taken. WC overcomes this problem and a pulse can propagate across the interface with no spurious reflections.

The discretized equation used to solve the wave for multiple grids is

$$\phi_{i,j}^{n+1} = 2\phi_{i,j}^{n} - \phi_{i,j}^{n-1} + \nu_i^2\delta_i^2\phi_{i,j}^{n} + \nu_j^2\delta_j^2\phi_{i,j}^{n} + \delta_n^{-}\left[\mu_i\delta_i^2\phi_{i,j}^{n} + \mu_j\delta_j^2\phi_{i,j}^{n}\right] - \delta_n^{-}\left[\varepsilon_i\delta_i^2\Phi_{i,j}^{n} + \varepsilon_j\delta_j^2\Phi_{i,j}^{n}\right] \qquad 4.8$$

where $\delta_i^2\phi_{i,j}^n = \phi_{i+1,j}^n - 2\phi_{i,j}^n + \phi_{i-1,j}^n$, $\delta_j^2\phi_{i,j}^n = \phi_{i,j+1}^n - 2\phi_{i,j}^n + \phi_{i,j-1}^n$, $\delta_n^- = f^n - f^{n-1}$, $\nu_i = \frac{c\Delta t}{\Delta x_{i,j}}$, $\nu_j = \frac{c\Delta t}{\Delta y_{i,j}}$, $\mu_i = \frac{\mu'\Delta t}{(\Delta x_{i,j})^2}$, $\mu_j = \frac{\mu'\Delta t}{(\Delta y_{i,j})^2}$, $\varepsilon_i = \frac{\varepsilon'\Delta t}{(\Delta x_{i,j})^2}$, $\varepsilon_j = \frac{\varepsilon'\Delta t}{(\Delta y_{i,j})^2}$ and $\frac{\varepsilon_i}{\mu_i} = \frac{\varepsilon_j}{\mu_j} = const.$. It must be noted that the ratio $\frac{\varepsilon}{\mu}$ over the entire domain is constant and therefore, the number of grid cells across the pulse remains constant.

At the grid interface,

$$\begin{aligned} \delta_x^2\phi_{i,j}^n &= \phi_{i+1,j}^n - 2\phi_{i,j}^n + \phi_{\text{Interface},j}^n \\ \delta_y^2\phi_{i,j}^n &= \phi_{i,j+1}^n - 2\phi_{i,j}^n + \phi_{i,\text{interface}}^n \end{aligned} \qquad 4.9$$

where values at the interface are calculated as shown in Figure 4.7a. A cylindrical wave that passes through the variable grid interface is shown in Figure 4.7b. It can be seen that there is almost no production of reflected waves from the interface. The total amplitude as the wave is passing through fine grid/ coarse grid interface is shown in Figure 4.8. This is checked for a range of grid ratios and presented in Figures 4.8a, 4.8b, 4.8c for grid ratios equal to 2, 4, 6 respectively. Anomalous numerical reflections during transition from the fine grid to the coarse grid can be suppressed by using variable confinement parameters, which are dependent on grid size and yet, the ratio $\frac{\varepsilon}{\mu}$ can be kept constant.

5. CARRIER FUNCTION

Developments that allow wave fronts to capture and propagate more details are described in this chapter. These details are required to compute interference. WC can be used to generate constant arrival time (Eikonal phase) surfaces accurately by storing the centroid arrival time at each grid point. Also, multiple-arrival times are easily accommodated, which is complicated using Eikonal schemes. Some recent developments in Eikonal methods [2] can treat multiple arrival times but, these methods require extra independent variables and complex data management schemes are used to control memory requirements. To demonstrate the ability of WC to capture these surfaces, arrival times for the wave fronts generated from a point source located at (128,128) on a 256×256 grid. The parameters used for this computation are $\nu = 0.23$, $\mu = 0.2$, $\varepsilon = 0.3$. The arrival time, $\hat{t}$, is calculated for the passage of each wave as

$$\hat{t}_{i,j} = \frac{\sum_n t\phi_{i,j}^n}{\sum_n \phi_{i,j}^n} \qquad 5.1$$

It can be seen in Figure 5.1a that the contours of arrival times are smooth with no stair-casing effects, which shows that there are no plottable discretization errors. The arrival times at the grid points in a cone with a range of angles, $\theta = 29^o - 32^o$, are compared to the exact values for validation purpose. For each i index, there are several grid points with varying j indices within the cone of $\theta = 29^o - 32^o$. The computed arrival times at each these grid points is plotted against exact values in Figure 5.1b. Assuming constant index of refraction, the exact arrival times are computed as

$$\hat{t}_{exact}(i,j) = \frac{r_{i,j}}{v}. \tag{5.2}$$

The direction of propagation, which is the gradient of the phase field, can also be accurately computed as

$$\vec{s}(s_x, s_y) = \frac{\bar{\nabla}\hat{t}_{i,j}}{|\nabla\hat{t}_{i,j}|}, \tag{5.3}$$

where s_x is the x-component of direction, and s_y is the y-component of direction. However, it is required that the wave front has entirely passed the grid point to accurately compute these properties. For very small wavelengths, the wave fronts and grid cells are hundreds of wavelengths wide and it becomes difficult to accommodate multiple arrival times when the waves are close to each other. To overcome that problem, the scalar field, ϕ, is used as a carrier function that can act as wave packet, which carries the required details of the propagating quantity. It is then not necessary for the wave front to entirely pass a grid point to capture the properties. The capability of WC is extended further using this "carrier" approach and numerous experiments are conducted.

5.1 Propagation Directions

The carrier approach is used to accurately propagate other properties of the wave with scalar function, ϕ. For example, to propagate the directions in 2D, the wave equation is solved three times for three quantities, ϕ, ϕs_x and ϕs_y as

$$\delta_n^2 \phi_l^n = v^2 \nabla^2 \phi_l^n + \mu \delta_n^- \left(\nabla^2 \phi_l^n\right) - \varepsilon \delta_n^- \left(\nabla^2 \Phi_l^n\right) \tag{5.4}$$

where l = 1, 2 and 3 and ϕ_l is defined as,

$$\begin{aligned} \phi_1 &= \phi \\ \phi_2 &= \phi s_x \\ \phi_3 &= \phi s_y . \end{aligned} \tag{5.5}$$

The updated directions are computed using the normalized relations,

$$s_x^{n+1} = \frac{\phi_2^{n+1}}{\sqrt{\left(\phi_2^{n+1}\right)^2 + \left(\phi_3^{n+1}\right)^2}} \tag{5.6}$$

$$s_y^{n+1} = \frac{\phi_3^{n+1}}{\sqrt{\left(\phi_2^{n+1}\right)^2 + \left(\phi_3^{n+1}\right)^2}}.$$

In the test computation described, the initial conditions for ϕ are given as

$$\begin{aligned} \phi_{i,j}^{n=0} &= A_0 \sec h\left[\gamma r_{i,j}\right] \\ \phi_{i,j}^{n=1} &= \frac{A_0}{A_1} \sec h\left[\gamma\left(r_{i,j} - \nu\right)\right] \end{aligned}, \qquad 5.7$$

with initial directions,

$$\begin{aligned} s_x &= \frac{i - i_0}{r_{i,j}} \\ s_y &= \frac{j - j_0}{r_{i,j}} \end{aligned}, \qquad 5.8$$

where the radius of the wave, $r_{i,j} = \sqrt{(i-i_0)^2 + (j-j_0)^2}$ with origin at the center of the domain (i_0, j_0). The parameters, ν, μ, and ε are the same for all three quantities and are $\nu = 0.23$, $\mu = 0.2$, and $\varepsilon = 0.3$. ϕ_1 and ϕ_2 behave as the scalar function itself during wave collision. In Figure 5.2, directions for the thin wave are shown at 4 different time steps. During interaction, directions temporarily are the mean values of the waves that are together. Then, they take their original forms after a short relaxation time.

5.2 Edge Diffraction

According to geometric optics, light travels in the form of rays and can bend in regions of non-uniformities in the medium. In isotropic media, the rays are normal to the primary wave fronts and fail to accommodate optical effects like diffraction. Since, diffraction was not described by the classical ray theory of light [30], it has been separately modeled using the Geometric Theory of Diffraction. On the other hand, Huygens principle (wave optics) postulates that every point on the wave front act as a point source for further propagation and can accurately account for diffraction. One such example is diffraction of a plane wave from a semi-infinite screen. The total field obtained by Sommerfeld [31] consists of incident, reflected and a cylindrical diffracted wave. According to Huygens principle, a secondary source is created at the edge and a part of the field from that source is transmitted into the non-illuminated (shadow). The incident field interferes with the diffracted field and interference fringes are observed in the illuminated region. At high frequency, the waves do not bend and maintain sharp shadows.

5.2.1 Keller's Approximation

The diffraction from a knife-edge can be computed using the Geometric Theory of Diffraction (GTD) developed by Joseph Keller [32] in the 1960s. It is an extension of geometric theory of

optics. This approximation will incorporate diffraction effects into the ray theory of light. Also, it introduces secondary sources that generate diffracted rays from the edges and corners of boundaries. GTD has been successfully applied in acoustics and Optics. Let us consider an incident field propagating horizontally that encounters a knife-edge, as shown in Figure 5.3b. The fundamental principle of GTD is that ray propagation is a local phenomenon. Furthermore, all fields of any origin obey the laws of geometric optics locally. The same is also true for diffracted rays. When the incident field is propagated in the direction normal to the edge, the diffracted field is cylindrical with the edge as its axis. Now, the total field at a point is the sum of all fields that pass through a point. An interference pattern is observed due to superposition of the geometric incident wave (u^i) and diffracted edge wave (u^D).

$$u = u^i + u^D \tag{5.9}$$

where

$$\begin{aligned} u^i &= A^i e^{i\omega t_i} \\ u^D &= D\frac{A^i}{r^{1/2}} e^{i\omega t_D} \end{aligned} \tag{5.10}$$

where ω is the frequency of the wave, r is the radius of the diffracted wave and D is the diffraction coefficient for the knife edge. The diffraction coefficient, D, developed by Keller is,

$$D = \frac{e^{i\pi/4}}{(2\pi k)^{1/2}\sin\theta}\left[\sin\left(\frac{\theta}{2}\right) + \cos\left(\frac{\theta}{2}\right)\right] \tag{5.11}$$

where θ is the angle between incident and diffracted rays, as shown in Figure 5.3b.

5.2.2 WC with Keller's Approximation

The high frequency approximation is achieved by WC (as a pde) by restricting the dissipation and contraction to the tangential and normal directions respectively. The incident wave propagation with a knife edge in the path has a sideward dissipation when computed using the equation,

$$\begin{aligned} \phi_{i,j}^{n-1} = 2\phi_{i,j}^{n} - \phi_{i,j}^{n-1} + \nu^2\left[\delta_x^2\phi_{i,j}^{n} + \delta_y^2\phi_{i,j}^{n}\right] + \mu\delta_n^-\left[\delta_x^2\phi_{i,j}^{n} + \delta_y^2\phi_{i,j}^{n}\right] \\ -\varepsilon\delta_n^-\left[\delta_x^2\Phi_{i,j}^{n} + \delta_y^2\Phi_{i,j}^{n}\right] \end{aligned} \tag{5.12}$$

As explained in Section 4.2, the nonlinear term acts as dissipation in the tangential direction to generate smooth wave fronts. Due to this effect, the arrival times start to bend as the wave encounters the edge, as shown in Figure 5.4. Even though this looks like diffraction, it actually is produced by dissipation from the confinement term to maintain the smooth field for ϕ.

The scalar function can be treated as a wave packet, which can be used to propagate other variables such as direction, as demonstrated in Section 5.1. This allows WC to capture the resulting incident wave produced by a knife edge without numerical spreading. The equation used for the high frequency approximation is

$$\phi_{i,j}^{n+1} = 2\phi_{i,j}^{n} - \phi_{i,j}^{n-1} + v^2\left[\delta_x^2\phi_{i,j}^{n} + \delta_y^2\phi_{i,j}^{n}\right] + \mu\delta_n^-\left[s_x\delta_x^2\phi_{i,j}^{n} + s_y\delta_y^2\phi_{i,j}^{n}\right] \\ -\varepsilon\delta_n^-\left[n_x\delta_x^2\Phi_{i,j}^{n} + n_y\delta_y^2\Phi_{i,j}^{n}\right] \qquad 5.13$$

where s_x and s_y are propagated as described in Section 5.1, the components of the normal direction are $n_x = -s_y$ and $n_y = s_x$. These waves obey the principles of geometric optics and are called geometric waves.

The arrival times of incident field, t^I, are computed using the relation given in equation (5.1). It can be seen in Figure 5.5a that a sharp shadow boundary is generated. The edge wave is propagated from a point source placed on the edge with the amplitude given by the incident field, A^I. The arrival times of the diffracted wave, t^D, are shown in Figure 5.5b. The total field is now calculated as

$$A = A^I\left(e^{i\omega t_1} + \frac{D}{\sqrt{r}}e^{i\omega t_2}\right). \qquad 5.14$$

The interference pattern is computed using the equation 5.11 and compared to the Fresnel far field approximation [30]. The intensity ratio, $\frac{I}{I_0}$, for planes, $i = 62$ and $i = 68$ is shown in Figure 5.6a and Figure 5.6b respectively. It can be seen that the results agree closely with the Fresnel far field approximation.

6 CONCLUSION

The wave equation is accurately solved using the newly developed, Wave Confinement method, which includes the realistic effects such as varying index of refraction, scattering from complex objects and interference. Unlike conventional Eulerian schemes, WC does not suffer from numerical dissipation and the properties such as total amplitude and centroid are conserved. It generates wave equation solutions as thin solitary waves that can persist on the grid indefinitely. WC involves a nonlinear term in the propagation equation, unlike the original linear wave equation. However, this nonlinear term in the WC does not produces amplitude exchange or phase shift during wave collisions. After collision, the waves take their correct speed and form after a short relaxation time. Also, the interactions behave in the same way in any dimension. This is an important property in capturing the effects of focusing, multiple scattering and all the cases where many waves simultaneously meet at a point.

WC has been shown to capture caustic regions with no additional steps in the computation process. It is also observed that WC in combination with Ray Tracing is accurate. This led to a new approximation called Eulerian/Lagrangian Transition. The smooth transition is observed even when there are irregular boundaries. In spite of having a nonlinear term in WC, the waves

are observed to focus with no shift in centroid positions. WC is also shown to generate smooth scattered surfaces during reflection from complex objects, preventing the need to use complicated adaptive grids. These objects are immersed in a Cartesian grid with no grid refinement and complex logic. This is due to the confinement term being diffusive in the tangential direction, keeping the scattered field smooth with no stair-casing effects. WC can also accommodate very small objects compared to the physical domain, and does not require fine grids, unlike conventional Eulerian schemes. This is an important feature in electromagnetic wave propagation in the atmosphere when complex surfaces such as terrain, buildings, etc., have to be accommodated.

Another important property of WC is its capability to capture the effects of varying index of refraction efficiently. This is an important feature in studying the effects of varying medium properties. Examples include evaporation or surface ducts (formed in atmosphere due to variations in density, temperature, etc), ionospheric ducts (formed in the ionosphere due to variations in electron density). These ducts can form caustic regions, multiple scattering etc. The confinement term is shown to treat such effects accurately and it is validated using Lagrangian method, which is an exact solution in high frequency approximation. Wave propagation across multiple grid interfaces is also proved to be accurate with no anomalous reflections. This will allow WC to use fine grids around an antenna and coarser grids in the far field. For the tested grid ratios, the transfer of amplitude across the interface is shown to be accurate.

WC is shown to accurately generate contours of constant arrival times as the wave passes a grid point. The scalar function propagated using WC can also be used as a carrier wave to propagate directions along with the wave. This allows efficient computation of the propagation directions. The properties propagated with the scalar function behave the same way as the scalar function itself during multiple interactions. Using the propagated directions, the wave solution in the high frequency approximation can be computed. When the wave encounters an edge, this will prevent sideward bending of the waves into the shadow region due to numerical diffusion. Using Keller's GTD along with WC, the diffraction pattern from a knife edge is computed and is shown to match quite well with the Fresnel far field approximation.

The local parabolic method is developed, which can compute propagation at any angle. It is an extension to the existing parabolic equation, which is confined to one preferred direction. Computations to simulate propagation at higher angles and single slit diffractions are done and validated using the exact analytical relations. Many computations are performed for a number of test cases and validated to check accuracy. The numerical properties of WC have to be well understood before using it for engineering applications. All the required validations have been performed for this new method to check the accuracy in actual complex conditions. WC still needs to be validated for propagation and interference effects for overlapping waves. As the pulsewidth will be relatively large compared to the wavelength in high frequency propagation, work has to be done to compute such effects within the wave. A more difficult, but widely studied challenge is the inverse scattering phenomena. This will be studied in the future to extend the applications of WC further.

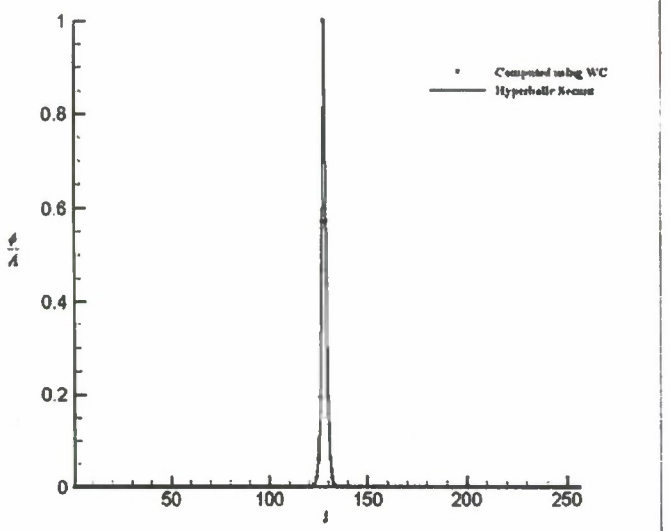

Figure 2.1: Pulse simulation using equation (2.30). The initial conditions for this computation are defined in equation (2.29).

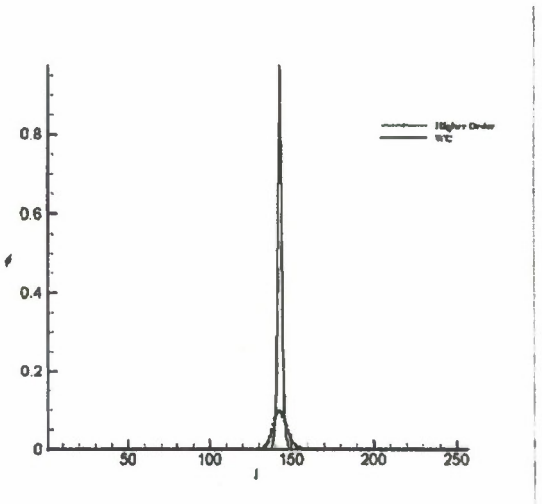

Figure 2.2: Comparison to higher order method. The pulse is propagated for 100 time steps using both WC and a higher order method.

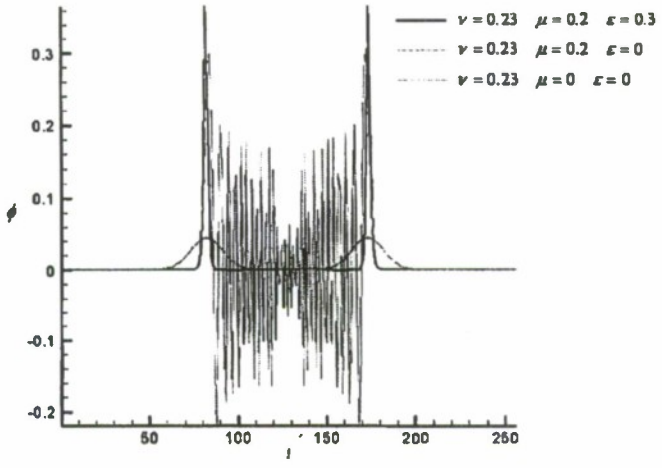

Figure 3.1: Behavior of 1D wave equation solution

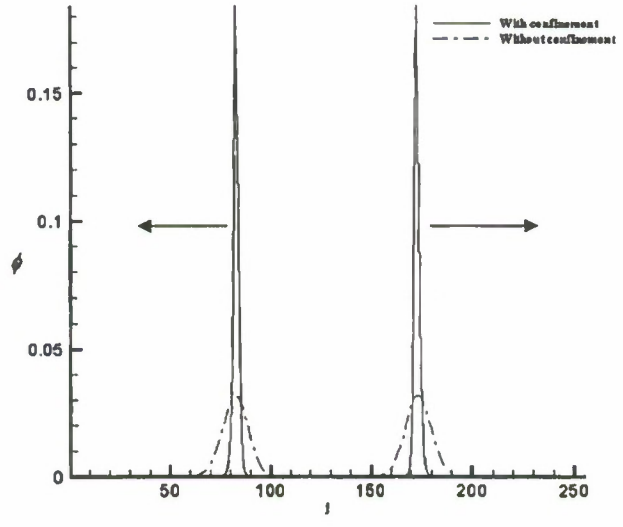

Figure 3.2: Computed pulses with and without confinement. The initial conditions are given in equation (3.5).

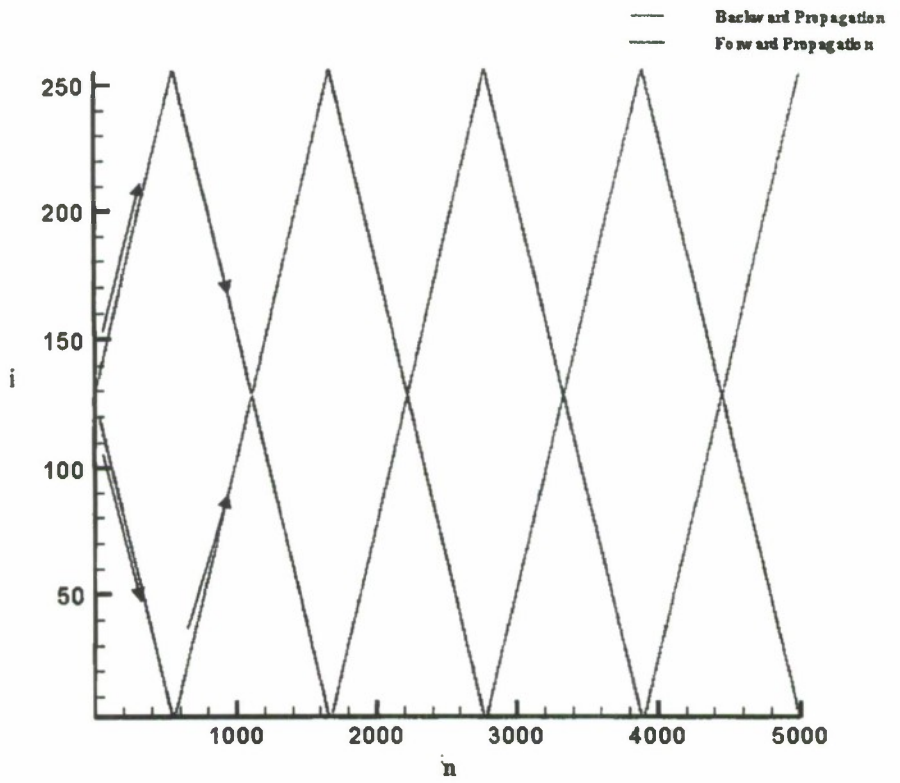

Figure 3.3: Centroid position.Collison of forward ($j + vn$) and backward ($j - vn$) propagating pulses with each other during propagation

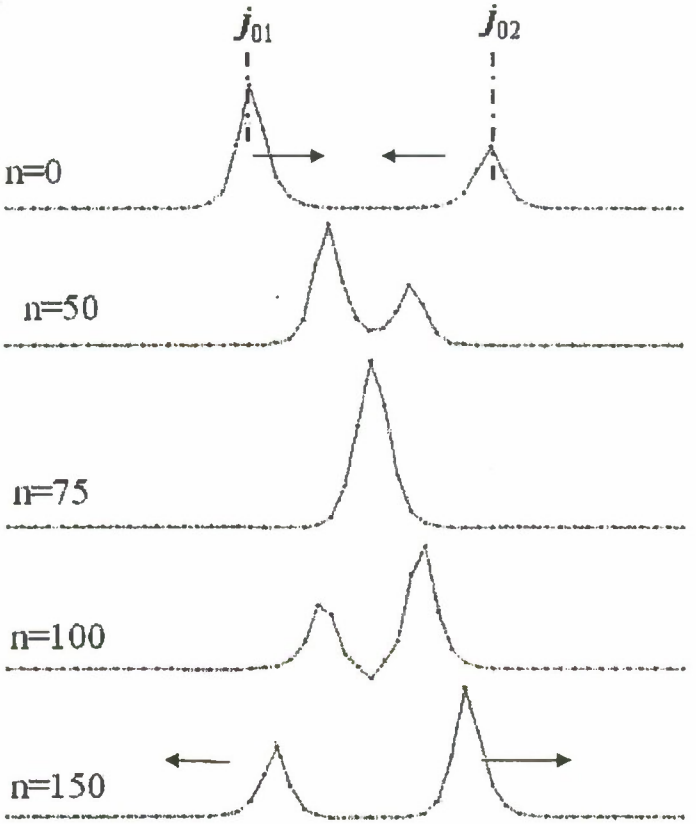

Figure 3.4: Interaction between two pulses of different amplitudes. The pulses undergo head-on collision during propagation for the intial conditions given in equation (3.10).

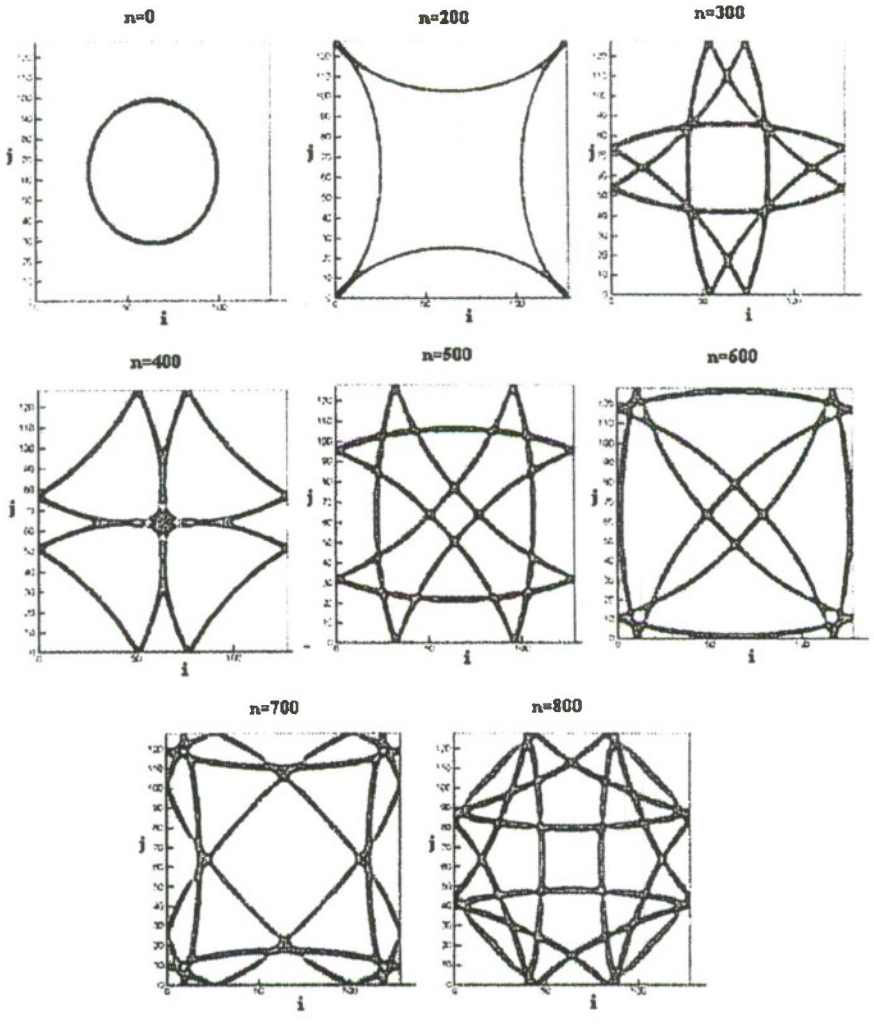

Figure 3.5 : Diverging circular wave front solved using equation (3.11)

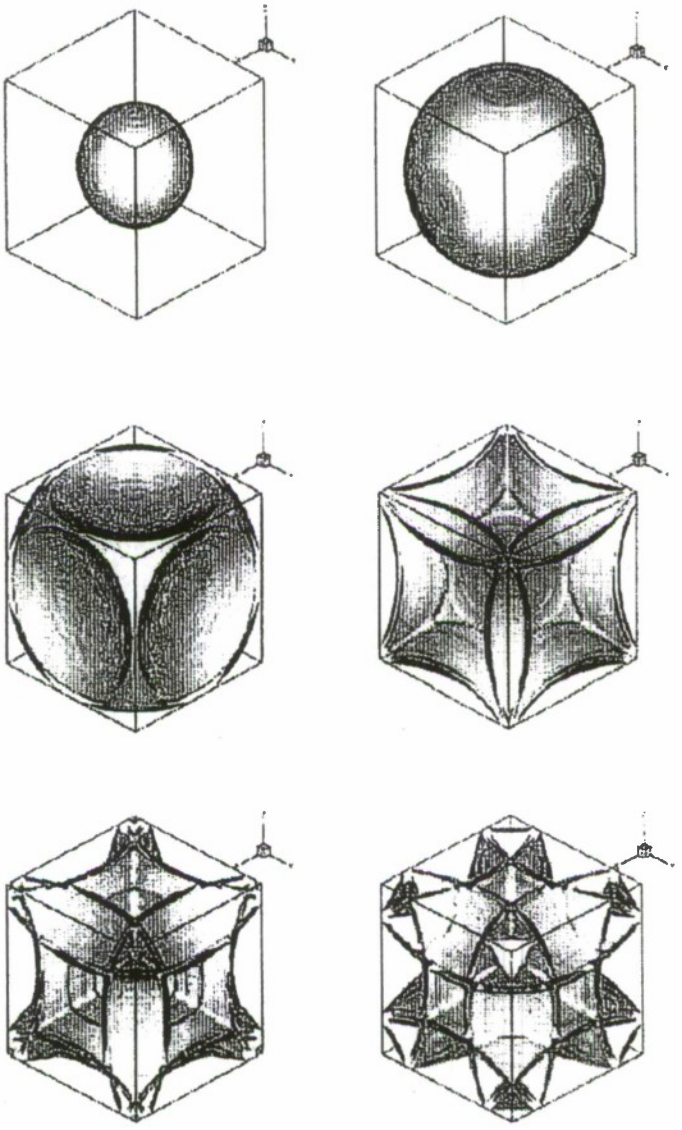

Figure 3.6: Spherical wave front propagation solved using equation (3.18)

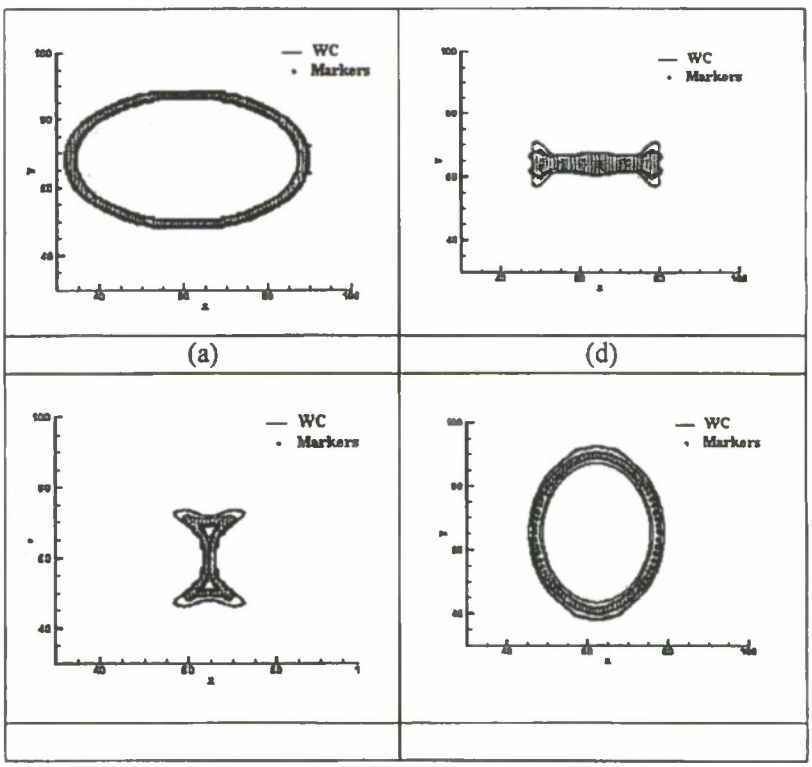

Figure 4.1: Inward propagating wave front computed using WC.
(a) n = 0, (b) n = 140, (c) n = 170, (d) n = 250

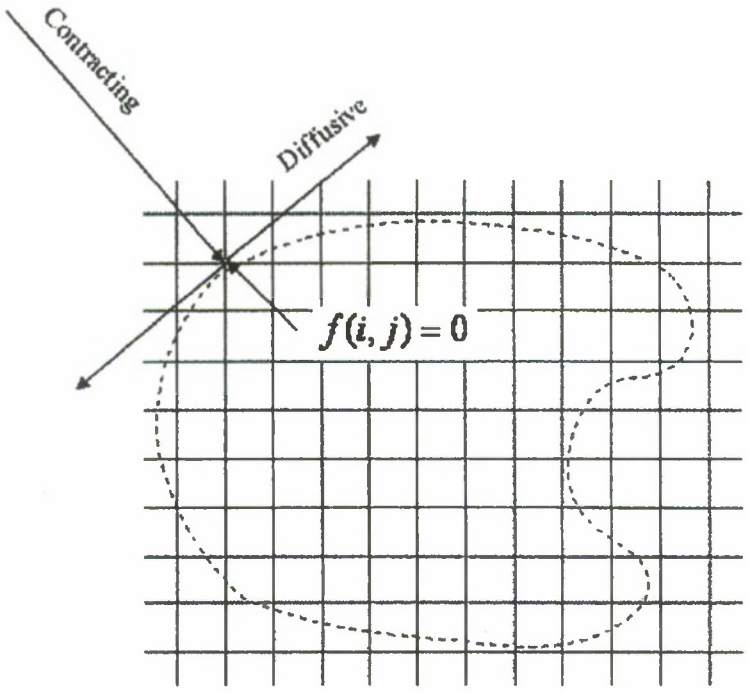

Figure 4.2: Immersed boundary to treat complex boundaries.

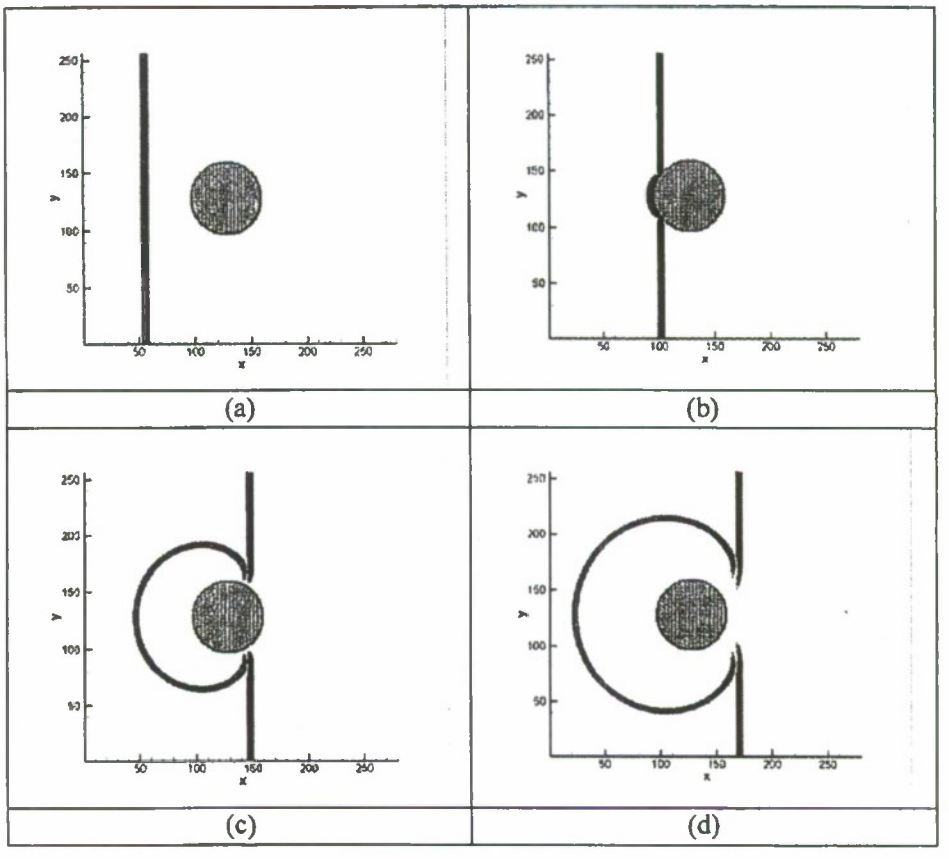

Figure 4.3: Scattering from Infinite Cylinder
(a) n = 0, (b) n = 200, (c) n = 400, (d) n = 600

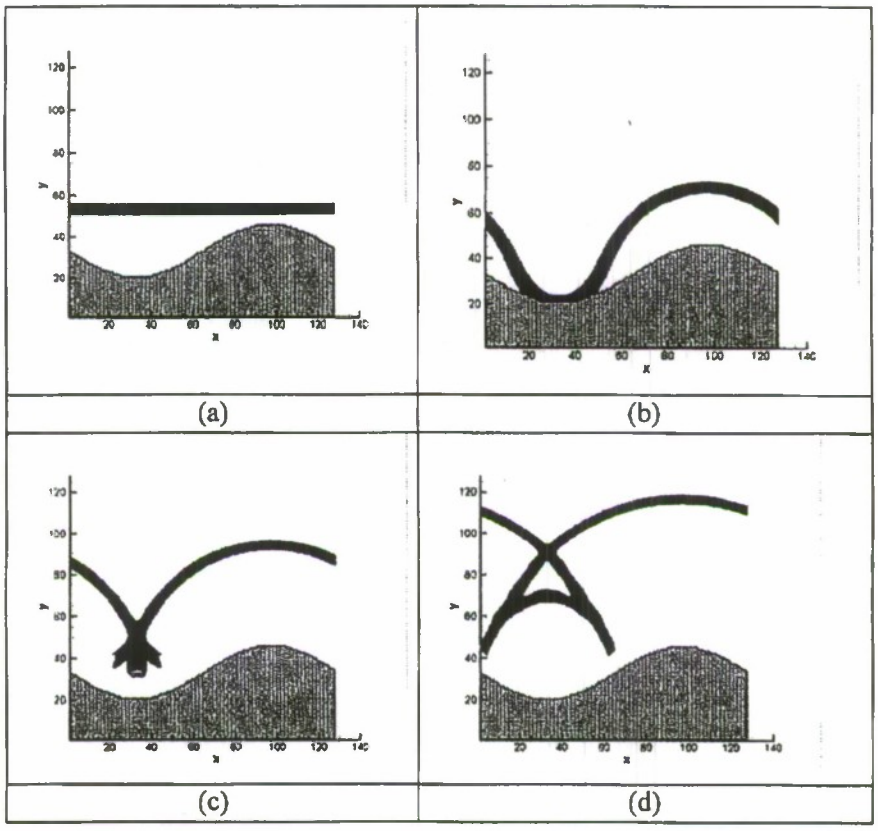

Figure 4.4: Reflection from the boundary with shape of a sine wave
(a) n = 0, (b) n = 200, (c) n = 300, (d) n = 500

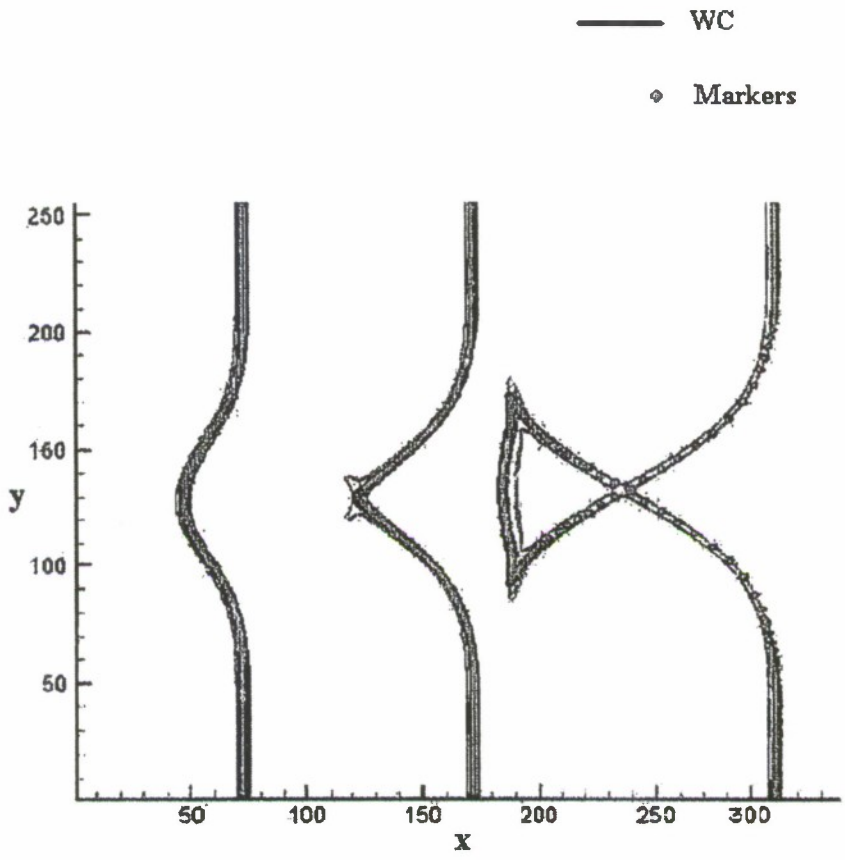

Figure 4.5: Varying index of refraction. The plane wave propagation across medium of profile given in equation 4.8

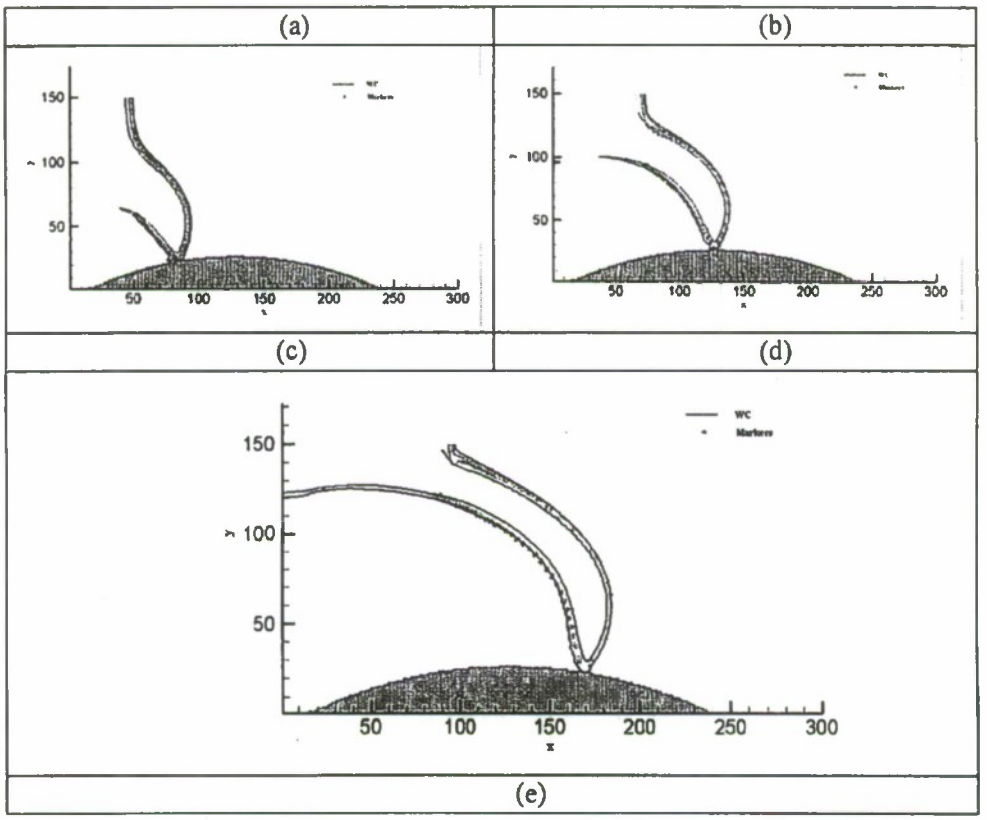

Figure 4.6: Plane wave propagation above curved surface, The medium has a diverging profile given equation (4.13) to imitate surface duct in atmosphere
(a) n = 0, (b) n = 200, (c) n = 400, (d) n = 600, (e) n = 800

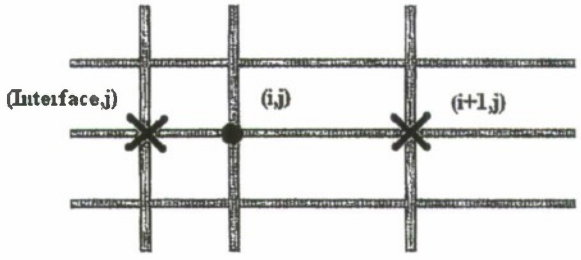

(a)

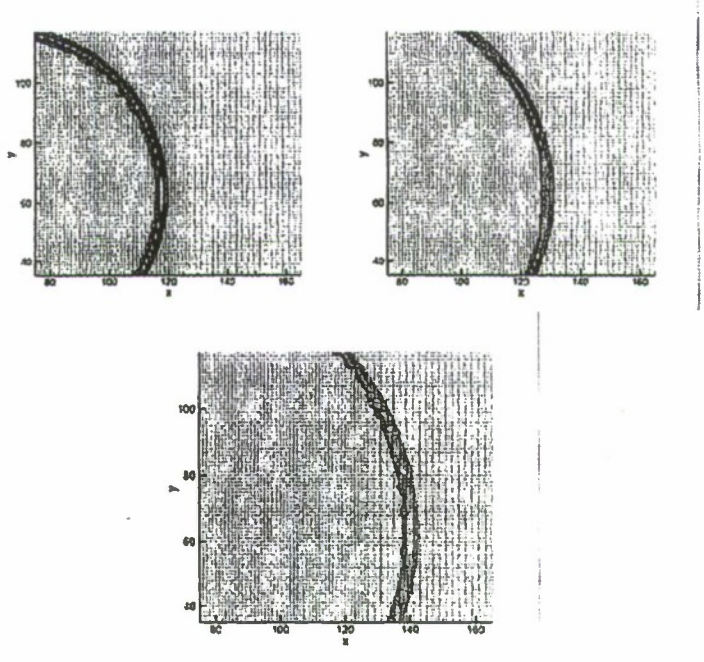

(b)

Figure 4.7: Multiple grids
(a) Computation of values at interface
(b) Circular wave front propagating across multiple grid interface

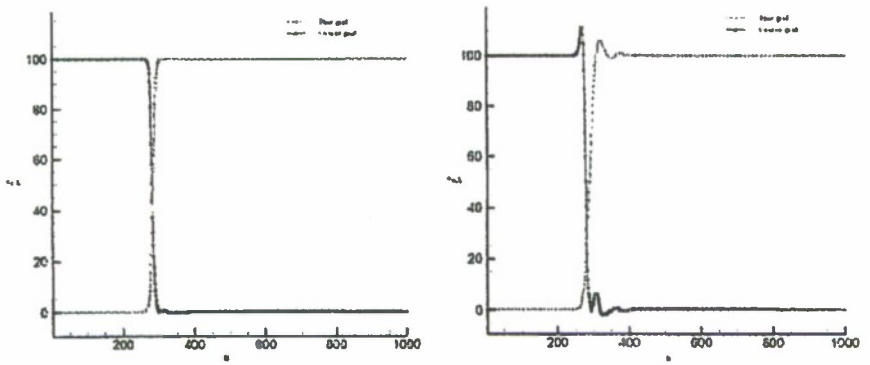

(a) (b)

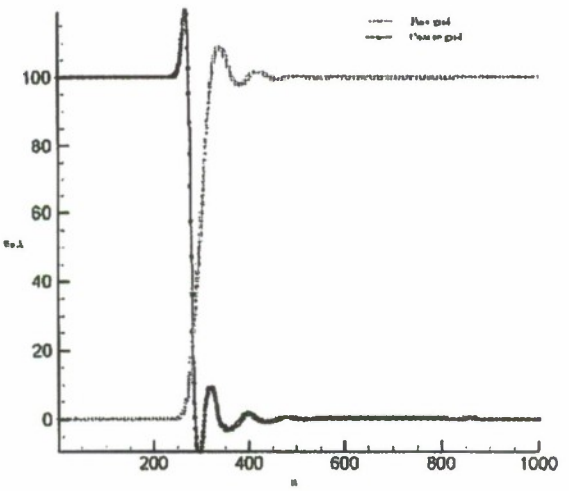

(c)

Figure 4.8: Amplitude transfer
(a) Grid ratio = 2
(b) Grid ratio = 4
(c) Grid ratio = 6

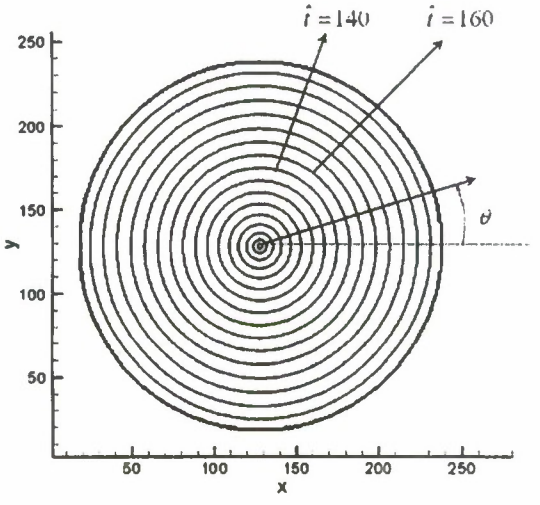

(a)

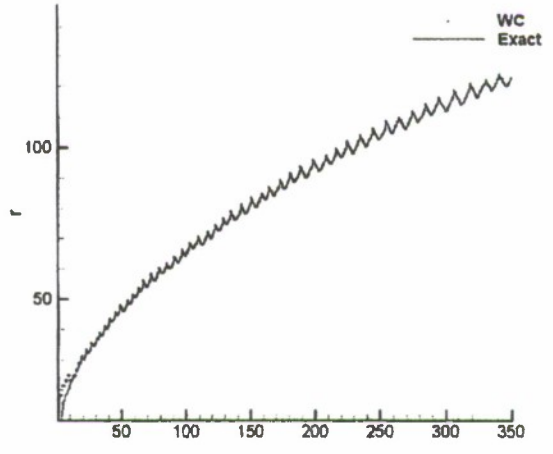

(b)

Figure 5.1:Arrival times of cylindrical wave generated from point source
(a) Contours of arrival time
(b) WC Vs Exact for $\theta = 29^{o} - 32^{o}$

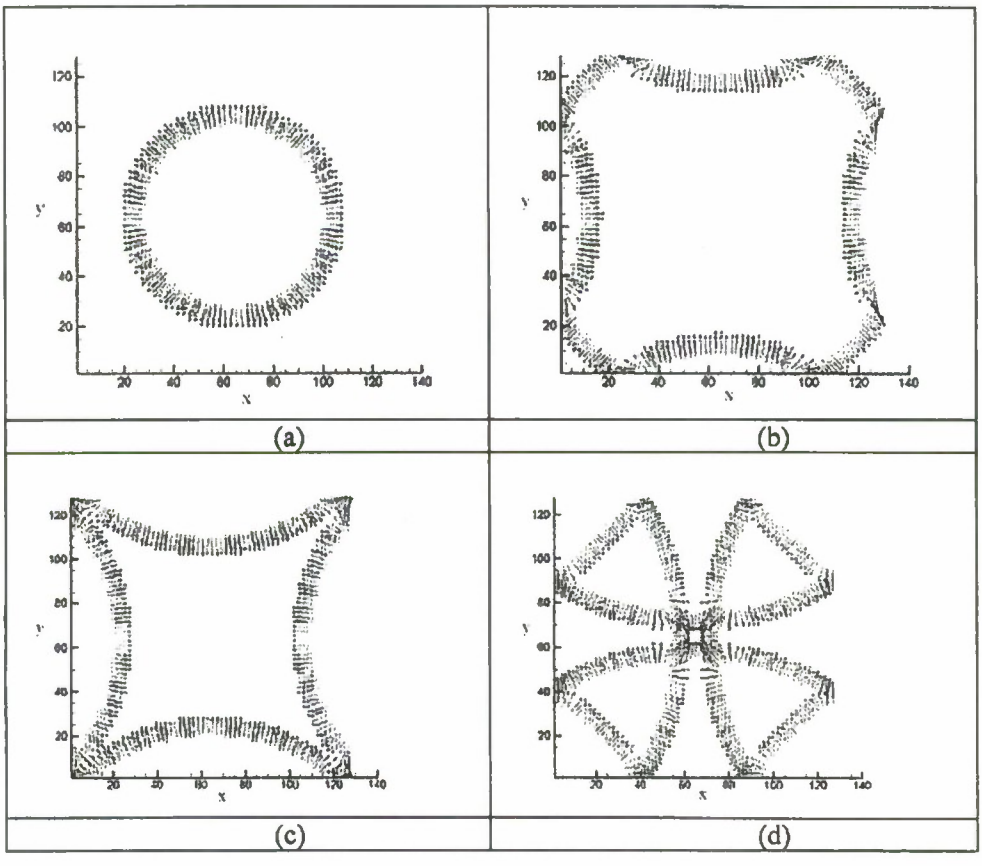

Figure 5.2: Propagation of directions

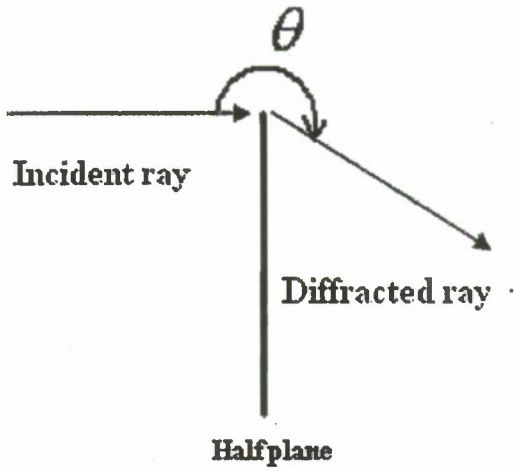

(b)
Figure 5.3: Knife edge diffraction
(a) Huygens principle
(b) Keller's geometric theory of diffraction

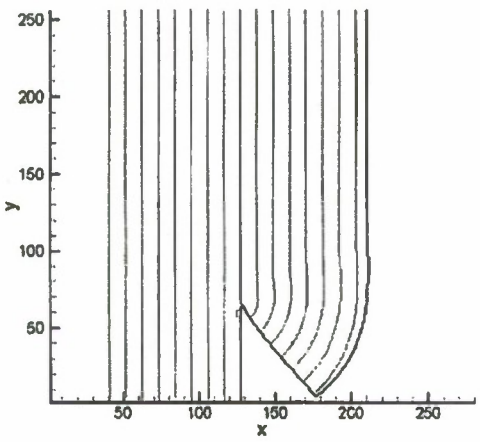

Figure 5.4 : Sideward bending of arrival time contours.

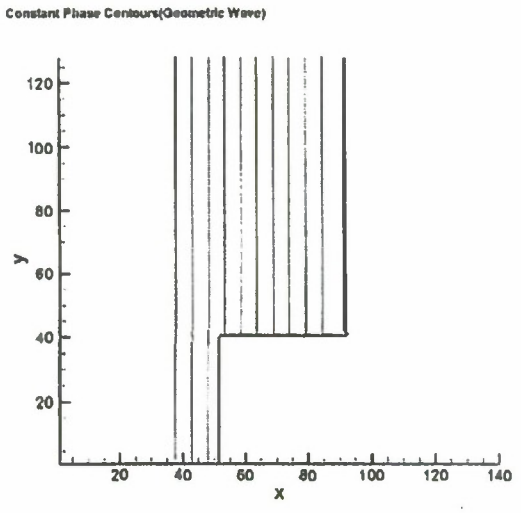

(a)

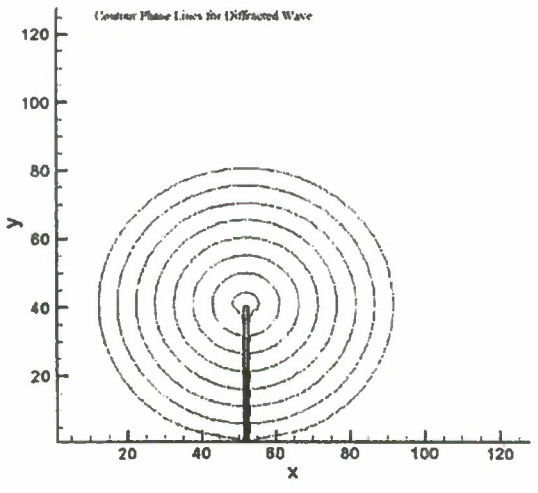

(b)

Figure 5.5: Arrival times for knife edge.
(a) Incident field t^i
(b) Diffracted field t^D

REFERENCES

1. Steinhoff, J., Wenren, Y., Underhill, D., and Puskas, E., "Computation of Short Acoustic Pulses", *Proceedings 6th International Symposium on CFD*, Lake Tahoe, September, 1995.
2. Anderson, D.A., Tannehill, J.C., and Pletcher, R.H., "Computational Fluid Mechanics and Heat Transfer", Hemisphere Publishing Corp., Washington D.C., USA, 1984.
3. Harten, A., "The Artificial Compression Method for Computation of Shocks and Contact Discontinuities III, Self-Adjusting Hybrid Schemes," *Mathematics of Computation*, 32(142), 363-389, 1978.
4. Rosenau, P., Hyman, J.M., Staley, M., "Multidimensional Compactons", *Physical Review Letters*, 98(2), 024101, 2007.
5. Smolarkiewicz, P. K., "A Simple Positive Definite Advection Scheme withSmall Implicit Diffusion" *Monthly Weather Review*, 111, 479-486, 1983.
6. Bishop, A.R., Krumhansl, J. A., Trullinger, S. E., "Solitons in Condensed Matter: A Paradigm", *Physica D: Nonlinear Phenomena*, 1(1), 1- 44, 1980.
7. Whitham, G.B., "Linear and Nonlinear Waves", Wiley Interscience, New York,1974.
8. Cahn, J.W., Hilliard, J.E., "Free Energy of a Nonuniform System. I. Interfacial Free Energy", *Journal of Chemical Physics*, 28(2), 258-267, 1958.
9. Kruskal, M.D., "The Korteweg–de Vries Equation and Related Evolution Equations", In: Nonlinear Wave Motion, *Lectures in Applied Mathematics*, 15 ,61–83, 1974.
10. Spencer, G.H., and Murty, M.V.R.K., "General Ray Tracing Procedure", *Journal of the Optical Society of America*, 52 (6), 672–678, 1962.
11. Bremmer, H., Lee, S.W., "Propagation of Geometric Optics Field in an Isotropic Inhomogeneous Medium", *Radio Science*, 19, 243-257, 1984.
12. Fatemi, E., Engquist, B., and Osher, S., "Numerical Solution of the High Frequency Asymptotic Expansion for the Scalar Wave Equation", *Journal of Computational Physics*, 120, 1995.
13. Benamou, J.D., Solliec, I., "An Eulerian Method for Capturing Caustics",*Journal of Computational Physics*, 162(1), 132-163, July, 2000.
14. Jin, S., Liub, H., Osher, S., and Tsai, R., "Computing Multi-valued PhysicalObservables for the High Frequency Limit of Symmetric Hyperbolic Systems", *Journal of Computational Physics*, 210(2), 497-518, December, 2005.
15. Born, M., and Wolf, E., "Principles of Optics", Cambridge University Press,Cambridge United Kingdom, 1999.
16. Sommerfeld, A., "Mathematische Theorie der Diffraction", *Math. Ann.*, 47, 317-374, 1896.
17. Keller, J.B., "Geometrical theory of diffraction", *Journal of Optical Society of America*, 52, 116-30, 1962.